

Hybrid Single Mode Nanophotonic-Plasmonic Waveguides for On-Chip Surface Enhanced Raman Spectroscopy

F. Peyskens¹, A. Dhakal¹, P. Van Dorpe², N. Le Thomas¹, and R. Baets¹,

¹Photonics Research Group, INTEC-department, Ghent University-imec; Center for Nano-and BioPhotonics, Ghent University, Technologiepark-Zwijnaarde 15, 9052 Ghent, Belgium

²imec, Kapeldreef 75, 3001 Heverlee, Belgium; Department of Physics, KULeuven, Celestijnenlaan 200D, 3001 Leuven, Belgium
frederic.peyskens@ugent.be

Abstract— We introduce a hybrid nanophotonic-plasmonic platform capable of generating Surface Enhanced Raman Spectroscopy signals from integrated bowtie antennas, excited and collected by a single mode silicon nitride waveguide. Moreover we discuss the relevant figure of merit, which represents the total Stokes power coupled into the fundamental waveguide mode for a given pump power, and outline strategies to optimize the Signal-to-Noise Ratio.

1. INTRODUCTION

Surface Enhanced Raman Spectroscopy (SERS) is a well-known technique to enhance Raman spectra by placing a resonant metallic nanostructure near the analyte under study. [1, 2] SERS signals are however mainly generated and collected by bulky and expensive microscopy systems. The development of photonic integrated circuits functionalized with dedicated nanoplasmonic structures would hence present a major step towards the realization of dense SERS probes, allowing multiplexed detection of extremely weak Raman signals. We have demonstrated for the first time such a hybrid platform where the SERS signal from integrated bowtie antennas, coated with a self-assembled monolayer of 4-nitrothiophenol (NTP), is excited and collected by a single mode silicon nitride waveguide (Fig. 1(a)). Due to the fully integrated nature of this single mode SERS-probe, one can rigorously quantify the complete enhancement and coupling process. [3] Below we will discuss the relevant figure of merit (*FOM*) of this new on-chip SERS platform and outline strategies to optimize the Signal-to-Noise Ratio (*SNR*).

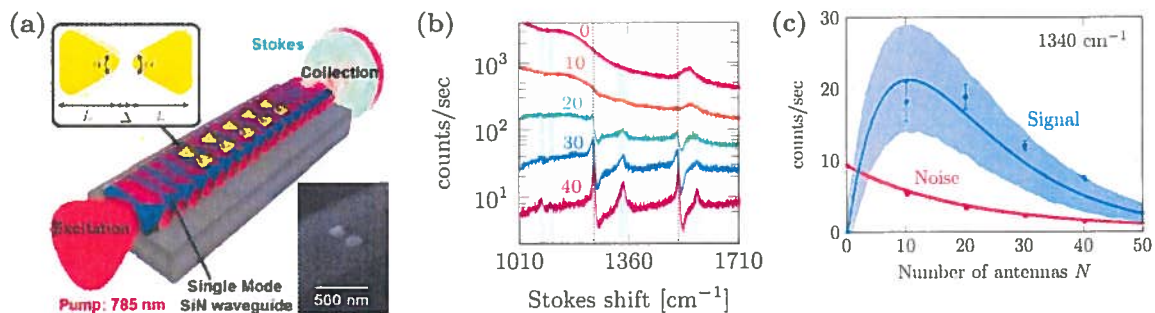


Figure 1: (a) Silicon nitride (SiN) waveguide functionalized with an array of N bowtie antennas. The bottom inset shows a SEM image of an integrated bowtie antenna. [3] (b) SERS spectra of waveguides functionalized with a varying number of N ($N = 0, 10, 20, 30, 40$) bowtie antennas with $\alpha \approx 60^\circ$, $L \approx 106 \pm 8$ nm and $\Delta \approx 48 \pm 13$ nm. [3] (c) Signal (blue) and shot noise (red) strength of the 1340 cm^{-1} peak as a function of N . The solid curve represents a fit of the experimental data to a theoretical model describing the on-chip SERS effects, developed in [3], while the shaded areas incorporate the theoretical impact of disorder in the system [3].

2. SIGNAL ENHANCEMENT AND NOISE REDUCTION

Figure 1(b) shows the Raman spectra obtained from waveguides functionalized with a different number of antennas N . The cyan shaded areas mark the spectral positions where an NTP Stokes peak is expected. The peaks denoted by the black dashed lines result from interference effects generated by the Au array. [3] While the non-functionalized ($N = 0$) reference waveguide does not generate any NTP SERS signal, it does have a large Raman background originating from the SiN core. The shot noise associated to this background will limit the detection of the smallest NTP features, but can be reduced by the attenuation caused by the nanoantennas if the waveguides are functionalized with a sufficiently large N (see Fig. 1(b)). While the dominant 1340

cm^{-1} peak is visible in all cases, the smallest 1110 cm^{-1} peak only appears for a sufficiently low background. In that respect the $N = 40$ waveguide exhibits a better performance as compared to the $N = 10$ case. However, the absolute signal strength of all the $N = 40$ peaks is lower than the $N = 10$ peaks as exemplified in Fig. 1(c) for the 1340 cm^{-1} peak. [3] Hence, there is a trade-off between signal enhancement and noise reduction, which in turn affects the SNR . In order to investigate this trade-off we developed an on-chip SERS model. Each antenna generates $\eta_A P_{pump}$ guided Stokes power, in both forward and backward direction, for a given pump power P_{pump} . The single antenna conversion efficiency η_A is an antenna dependent factor incorporating the integrated field enhancement profile near the metal surface. The total forward propagating Stokes power generated by an array of N coated antennas was shown to be proportional to $FOM_F = \eta_A e_S^{(1-N)} (1 - (e_S/e_P)^N) (1 - e_S/e_P)^{-1}$. The additional array factor results from the combined extinction of pump (e_P) and Stokes (e_S) light due to all the antennas. The background on the other hand is proportional to $FOM_{bg} = \eta_{bg} L_1 (e_P^{-N} + e_S^{-N})$ in which η_{bg} is a waveguide dependent factor incorporating the specific modal field profile and $2L_1$ is the total length of the waveguide. Finally, the SNR is then proportional to $SNR \propto FOM_F / \sqrt{FOM_F + FOM_{bg}}$. [3]

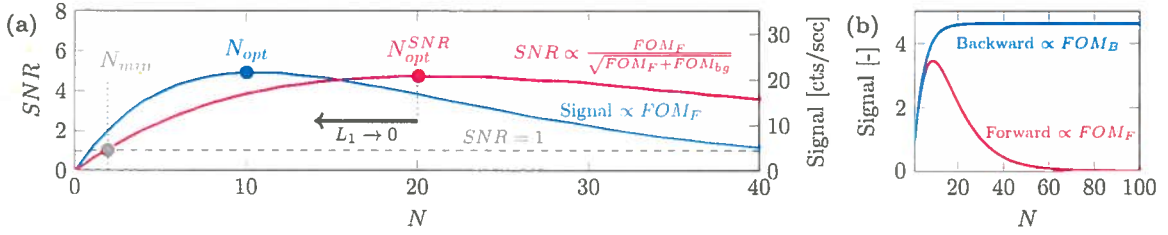


Figure 2: (a) Signal and SNR as a function of N for the 1340 cm^{-1} peak of Fig. 1(c). (b) Comparison between Forward and Backward on-chip SERS scattering for $e_P = 1.16$ and $e_S = 1.10$.

The experimental signal strength and corresponding SNR of the 1340 cm^{-1} peak are shown in Fig. 2(a). One can see that if $N < N_{min}$, detection is not possible because $SNR < 1$. The signal is maximal for $N = N_{opt}$ while the SNR is maximal for $N_{opt}^{SNR} > N_{opt}$. This exemplifies the trade-off between signal enhancement and noise reduction. It should be noted however that the SERS signal originates from a relatively short section (which can be made as short as $\approx 10 \mu\text{m}$ for a single antenna) as compared to the total length $2L_1$ ($\approx 10000 \mu\text{m}$ in our experiment) which is responsible for the large background. By sufficiently reducing L_1 ($L_1 \rightarrow 0$), the trade-off relaxes because one maintains the possibility to select an antenna number which maximizes FOM_F while achieving the maximum SNR at the same time (i.e. $N_{opt}^{SNR} \rightarrow N_{opt}$). Furthermore, one can gain in absolute signal strength by collecting the backward propagating SERS light because the backscattered signal from the first antenna, which is the strongest, is still fully available at the output. The signal from subsequent antennas then experiences an ever increasing attenuation by the previous antennas, such that the signal eventually saturates for a sufficiently large number of antennas (see Fig. 2(b)). By applying similar reasonings as in [3], one can show that the backward propagating SERS signal is proportional to $FOM_B = \eta_A (1 - (e_P e_S)^{-N}) (1 - (e_P e_S)^{-1})^{-1}$. The highest SERS signal S_{max} that can be collected from this hybrid platform is hence given by $S_{max} = \eta_A (1 - 1/(e_P e_S))^{-1}$ for a given antenna geometry. When one eventually is limited to the shot noise of the SERS signal (i.e. $FOM_B \gg FOM_{bg}$), the highest possible SNR is proportional to $SNR_{max} \propto \sqrt{\eta_A (1 - 1/(e_P e_S))^{-1}}$. Currently we are working on dedicated on-chip Y-splitters which decouple the pump beam from the waveguide carrying the SERS signal in order to reduce the background signal. Moreover, the backscattered light is collected in such a Y-splitter configuration to improve on the absolute signal strength. Initial experiments show that the background can be reduced by a factor 100 (shot noise reduction by 10) compared to the background of simple straight waveguides (for the same pump power). So the SNR is expected to increase by at least 10.

Improved chip designs are expected to push towards the $N_{min} = 1$ limit, such that signals from a single antenna can be detected, and could ultimately enable quantitative and multiplexed detection of several biological and chemical substances, such as viruses or DNA, on a fully integrated platform.

REFERENCES

1. Anker, J. N., et al. "Biosensing with plasmonic nanosensors," *Nat. Mater.*, Vol. 7, 442-453, 2008.
2. Halas, N. J., et al. "Plasmons in strongly coupled metallic nanostructures," *Chem. Rev.*, Vol. 111, 3913-3961, 2011.
3. Peyskens, F., et al. "Surface Enhanced Raman Spectroscopy Using a Single Mode Nanophotonic-Plasmonic Platform," *ACS Photonics*, Vol. 3(1), 102-108, 2016.

META'16 Malaga - Spain

The background of the cover is a dark, textured grey. Overlaid on this are numerous bright blue lines of varying thickness and length, some straight and some curved, creating a sense of motion and depth. Small white dots are scattered throughout, often at the ends of the blue lines, resembling a starry field or a network of nodes.

The 7th International Conference on Metamaterials, Photonic Crystals and Plasmonics

Proceedings

ISSN 2429-1390

metaconferences.org

Designing broadband silicon devices using subwavelength structures (pp. 399)

Robert Halir, Jose Manuel Luque-Gonzalez, Shurui Wang, Alejandro Sanchez-Postigo, Juan Wanguemert-Perez, Pavel Cheben, Jens Schmid, Dan-Xia Xu, Siegfried Janz, Jean Lapointe,

Transfer printing approach to fabricate adaptable, self-standing and high efficiency polymer solar cells (pp. 401)

Silvia Colodrero, Pablo Romero-Gomez, Paola Mantilla-Perez, Jordi Martorell,

Annealing Studies of Gold Plasmonic Nanostructured Arrays (pp. 403)

Matthew Nicholson, Robert Bowman, Antony Murphy, Robert Pollard,

Active modulation of visible light with graphene-loaded ultrathin metal plasmonic antennas (pp. 405)

Renwen Yu, Valerio Pruneri, Javier Garcia de Abajo,

Highly-responsive subwavelength plasmonic photodetector for silicon nanophotonics (pp. 407)

Igor A. Khramtsov, Dmitry Yu. Fedyanin,

Plasmonic materials for hot carrier devices (pp. 409)

Jeremy Munday,

Enhanced optical nonlinearities in periodic photonic nanostructures containing patterned graphene and other 2D materials (pp. 410)

Nicolae Panoiu, Martin Weismann,

Quantum efficiency gains by metal nanostructures in organic and quantum dot solar cells (pp. 411)

Jung-Yong Lee, Doh Chang Lee,

Interactions between organic excitons and plasmonic metasurfaces (pp. 413)

Deirdre M. O'Carroll, Zeqing Shen, Christopher Petoukhoff, Katsuya Noji, Ankur Dalsania,

Plasmonic resonances in gold nanorod-film coupled system (pp. 414)

Xingxing Chen, Richard Blaikie, Boyang Ding, Min Qiu,

Selecting a Plasmonic Material Using a Two-Dimensional Analysis of Confinement and Propagation Length (pp. 416)

Babak Dastmalchi, Thomas Koschny, Costas M. Soukoulis, Philippe Tassin,

Non-Hermitian Wave Mixing (pp. 417)

Ramy El-Ganainy, J. I. Dadap, R. M. Osgood Jr.,

Multiphysics simulation of tunable and frequency selective metamaterial absorbers (pp. 419)

Amy Liu, Ahsan Alam, Jens Niegemann, James Pond,

Observation of topologically protected edge states in arrays of evanescently coupled plasmonic waveguides (pp. 421)

Stefan Linden, Felix Bleckmann, Andrea Alberti,

New Trends in Computational Photonics (pp. 422)

Salah Sabry Obayya,

Hybrid Single Mode Nanophotonic-Plasmonic Waveguides for On-Chip Surface Enhanced Raman Spectroscopy (pp. 424)

Frederic Peyskens, Ashim Dhakal, Pol Van Dorpe, Nicolas Le Thomas, Roel Baets,